

Department of Atmospheric Sciences, National Central University
Chair Professor Lectures supported by the MOST, Taiwan

Dynamical Mountain Meteorology

Dr. Yuh-Lang Lin, ylin@cat.edu; <http://mesolab.ncat.edu>
North Carolina A&T State University
(Ref.: *Mesoscale Dynamics*, Y.-L. Lin, Cambridge, 2007)

Chapter 11 Flows over Larger Mesoscale Mountains

(Based on Sec. 5.5 of Lin 2007)

Table of Contents:

- 11.1 Rotational Effects
- 11.2 Lee Cyclogenesis
- 11.3 Orographic Influence on Cyclone Tracks

11.1 Rotational effects

- In the previous sections, effects of Earth's rotation are neglected. This is approximately valid for flow with Rossby number ($R_o = U/fL$, where L is the horizontal scale of the mountain) much larger than 1.
- However, for flow over mountains with $R_o = O(1)$ or smaller, the effects of Earth's rotation cannot be ignored.
- In this situation, the advection time (L/U) for an air parcel to pass over the mountain is too large to be ignored compared to the period of inertial oscillation due to Earth's rotation ($2\pi/f$).
- Flow past many mesoscale mountain ranges, such as the European Alps, US Rockies, Canadian Rockies, Andes, the Scandinavian mountain range, the New Zealand Alps, and the Central Mountain Range of Taiwan, belong to this category.

- For flow over a very broad large-scale mountain, which gives a very small Rossby number (e.g., $R_o \leq 0.2$), the flow can be approximated by the quasi-geostrophic theory.
- In general, however, for flow over mesoscale mountains, the Rossby numbers are on the order of 1, for which the influence of the Coriolis force is too large to be ignored, but too small to be approximated by the quasi-geostrophic theory.
- In considering the small-amplitude, two-dimensional ($\partial/\partial y = 0$), steady state, inviscid, rotating, uniformly stratified, Boussinesq flow over an infinitely long ridge on an f -plane, the governing equations can be derived from (3.6.1)-(3.6.5),

$$\left(U^2 \frac{\partial^2}{\partial x^2} \right) \left(\frac{\partial^2 w'}{\partial x^2} + \frac{\partial^2 w'}{\partial z^2} \right) + f^2 \frac{\partial^2 w'}{\partial z^2} + N^2 \frac{\partial^2 w'}{\partial x^2} = 0. \quad (5.5.1)$$

Similar to the procedure for obtaining solutions described in subsection 5.2.1, the vertical displacement can be obtained by,

$$w'(x, z) = 2 \operatorname{Re} \left[\int_0^l ikU \hat{h}(k) e^{i\sqrt{l^2-k^2}z} e^{ikx} dk + \int_l^\infty ikU \hat{h}(k) e^{-\sqrt{k^2-l^2}z} e^{ikx} dk \right] \quad (5.2.4)$$

$$\eta(x, z) = 2 \operatorname{Re} \left[\int_0^\infty \hat{h}(k) e^{i(kx+mz)} dk \right], \quad (5.5.2)$$

where $\hat{h}(k)$ is the one-sided Fourier transform of the mountain shape $h(x)$ (Appendix 5.1)

$$\hat{h}(k) = \frac{1}{2\pi} \int_{-\infty}^\infty h(x) e^{-ikx} dx, \quad (5.5.3)$$

and m is the vertical wave number

$$m = \sqrt{\frac{k^2(N^2 - k^2U^2)}{k^2U^2 - f^2}}. \quad (5.5.4)$$

Note that (5.5.4) is similar to that defined in (3.6.10), in which $\Omega \equiv \omega - kU$ for a time-dependent problem.

Several regimes exist for the mountain waves in a rotating stratified atmosphere, similar to those of inertial gravity waves discussed in Chapter 4 and summarized in Table 3.2.

Table 3.2: Dispersion relations and approximated equations of w' for mesoscale waves in different flow regimes

The governing equation for a linear, adiabatic, Boussinesq flow with a uniform basic state wind (U) and stratification (N) can be written:

$$\left(\frac{\partial}{\partial t} + U \frac{\partial}{\partial x}\right)^2 \left(\frac{\partial^2 w'}{\partial x^2} + \frac{\partial^2 w'}{\partial y^2} + \frac{\partial^2 w'}{\partial z^2}\right) + f^2 \frac{\partial^2 w'}{\partial z^2} + N^2 \left(\frac{\partial^2 w'}{\partial x^2} + \frac{\partial^2 w'}{\partial y^2}\right) = 0. \quad (3.6.6)$$

The dispersion relation is

$$m^2 = \frac{K^2(N^2 - \Omega^2)}{\Omega^2 - f^2}; \quad \Omega = \omega - kU, \quad (3.6.10)$$

and three major flow regimes are

(I) High-frequency evanescent flow regime ($\Omega^2 > N^2 > f^2$; m imaginary)

(i) Potential (irrotational) flow ($\Omega^2 \gg N^2 > f^2$)

$$m^2 \approx -K^2; \quad \left(\frac{\partial}{\partial t} + U \frac{\partial}{\partial x}\right)^2 \left(\frac{\partial^2 w'}{\partial x^2} + \frac{\partial^2 w'}{\partial y^2} + \frac{\partial^2 w'}{\partial z^2}\right) = 0, \quad (3.6.12)$$

(i) Nonrotating evanescent flow ($\Omega^2 > N^2 \gg f^2$ and $O(\Omega) = O(N)$)

$$m^2 \approx -K^2 \left(1 - \frac{N^2}{\Omega^2}\right); \quad \left(\frac{\partial}{\partial t} + U \frac{\partial}{\partial x}\right)^2 \left(\frac{\partial^2 w'}{\partial x^2} + \frac{\partial^2 w'}{\partial y^2} + \frac{\partial^2 w'}{\partial z^2}\right) + N^2 \left(\frac{\partial^2 w'}{\partial x^2} + \frac{\partial^2 w'}{\partial y^2}\right) = 0$$

(II) Vertically propagating wave regime ($N^2 > \Omega^2 > f^2$; m real)

(i) Pure gravity waves ($N^2 > \Omega^2 \gg f^2$ and $O(N) = O(\Omega)$)

$$m^2 \approx K^2 \left(\frac{N^2}{\Omega^2} - 1\right); \quad \left(\frac{\partial}{\partial t} + U \frac{\partial}{\partial x}\right)^2 \left(\frac{\partial^2 w'}{\partial x^2} + \frac{\partial^2 w'}{\partial y^2} + \frac{\partial^2 w'}{\partial z^2}\right) + N^2 \left(\frac{\partial^2 w'}{\partial x^2} + \frac{\partial^2 w'}{\partial y^2}\right) = 0 \quad (3.6.14)$$

(ii) Hydrostatic gravity waves ($N^2 \gg \Omega^2 \gg f^2$)

$$m^2 = \left(\frac{KN}{\Omega}\right)^2; \quad \left(\frac{\partial}{\partial t} + U \frac{\partial}{\partial x}\right)^2 \frac{\partial^2 w'}{\partial z^2} + N^2 \left(\frac{\partial^2 w'}{\partial x^2} + \frac{\partial^2 w'}{\partial y^2}\right) = 0, \quad (3.6.16)$$

(iii) Hydrostatic inertia-gravity waves ($N^2 \gg \Omega^2 > f^2$ and $O(\Omega) = O(f)$)

$$m^2 = \frac{K^2 N^2}{\Omega^2 - f^2}; \quad \left[\left(\frac{\partial}{\partial t} + U \frac{\partial}{\partial x}\right)^2 + f^2\right] \frac{\partial^2 w'}{\partial z^2} + N^2 \left(\frac{\partial^2 w'}{\partial x^2} + \frac{\partial^2 w'}{\partial y^2}\right) = 0, \quad (3.6.18)$$

(III) Low-frequency evanescent flow regime ($N^2 > f^2 > \Omega^2$; m imaginary)

(i) Quasi-geostrophic flow ($N^2 > f^2 \gg \Omega^2$)

$$m^2 \approx \frac{-K^2 N^2}{f^2}; \quad f^2 \frac{\partial^2 w'}{\partial z^2} + N^2 \left(\frac{\partial^2 w'}{\partial x^2} + \frac{\partial^2 w'}{\partial y^2}\right) = 0. \quad (3.6.20)$$

- We have already discussed two flow regimes in earlier sections, such as the *nonrotating evanescent flow regime* for $k^2 U^2 > N^2 \gg f^2$, and the *nonrotating vertically propagating wave regime* for $N^2 > k^2 U^2 \gg f^2$.
- To demonstrate the rotational effects, we consider an extreme case of a flow past a very broad mountain ridge.

Assuming a bell-shaped mountain range, (5.2.5), its Fourier transform can be obtained:

$$\hat{h}(k) = \frac{h_m a}{2} e^{-ka}, \quad \text{for } k > 0. \quad (5.2.6)$$

In this situation, we have $N^2 > f^2 \gg k^2 U^2$ and the vertical wave number reduces to $m = ikN/f$. As discussed in Chapter 4, this is equivalent to making the quasi-geostrophic approximation.

Substituting $\hat{h}(k)$ and m into (5.5.2) leads to the solution for a quasi-geostrophic flow over a very broad bell-shaped mountain ridge,

$$\eta(x, z) = \frac{h_m a^2 (Nz/fa + 1)}{x^2 + a^2 (Nz/fa + 1)^2}. \quad (5.5.5)$$

- The above solution can be extended to quasi-geostrophic flow over a three-dimensional, isolated mountain, as shown in Fig. 5.26a.

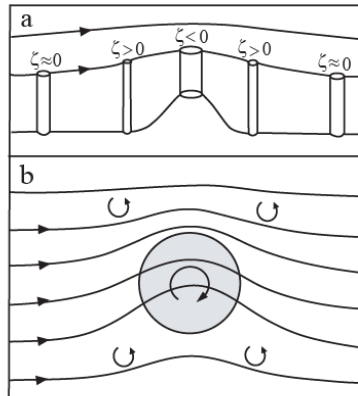


Fig. 5.26: A sketch of a quasi-geostrophic, stratified flow over a circular mountain. (a) The vertical vorticity associated with the deformation of vortex tubes is shown. The solid lines represent trajectories on the vertical cross section through the center of the mountain. (b) The streamline pattern near the surface for the flow associated with (a) as seen from above. (Lin 2007, Adapted from Smith 1979 and Buzzi and Tibaldi 1977)

The lifting of θ – surfaces aloft is less than the mountain height, but the lifting is more widespread.

Assuming a non-rigid lid top boundary, the air column upstream of the mountain is stretched slightly, producing weak cyclonic vorticity.

Over the mountain, the air column is shortened producing anticyclonic vorticity. This anticyclonic vorticity is associated with a mountain-induced high pressure or anticyclone.

On the lee side, the air column is slightly stretched again, producing weak cyclonic vorticity.

Figure 5.26b shows the streamline pattern near the surface on a horizontal plane for the flow associated with Fig. 5.26a.

When a straight incoming flow approaches a mountain ridge in the Northern Hemisphere, it turns cyclonically (left facing downstream)

slightly upstream of the mountain, anticyclonically over the mountain, and cyclonically slightly on the immediate lee side in response to the slight vorticity stretching, major vorticity shrinking, and slight vorticity stretching of the vertical vorticity, in order to conserve the potential vorticity (Fig. 5.26a).

This gives the streamline pattern as depicted in Fig. 5.26b. The perturbation velocity and pressure field decay away from the mountain. The upwarping of isentropic surfaces and the cold-core anticyclone near the ground, caused by a cold air mass at the surface, is analogous to a mountain anticyclone.

When a preexisting cyclone passes over a mountain, its low pressure or cyclonic vorticity is weakened by the mountain-induced high pressure or even completely suppressed the low (filled in) on a weather map. After it passes over the mountain, the cyclone reappears on the lee side. In addition, the cyclone track is often deflected by the mountain-induced anticyclone. This will be addressed in the next subsection.

- Due to mathematical intractability, asymptotic methods or numerical techniques are often employed to solve (5.5.2). Figure 5.27 shows an asymptotic solution of (5.5.2) multiplied by the non-Boussinesq factor $\sqrt{\rho_s / \rho(z)}$.

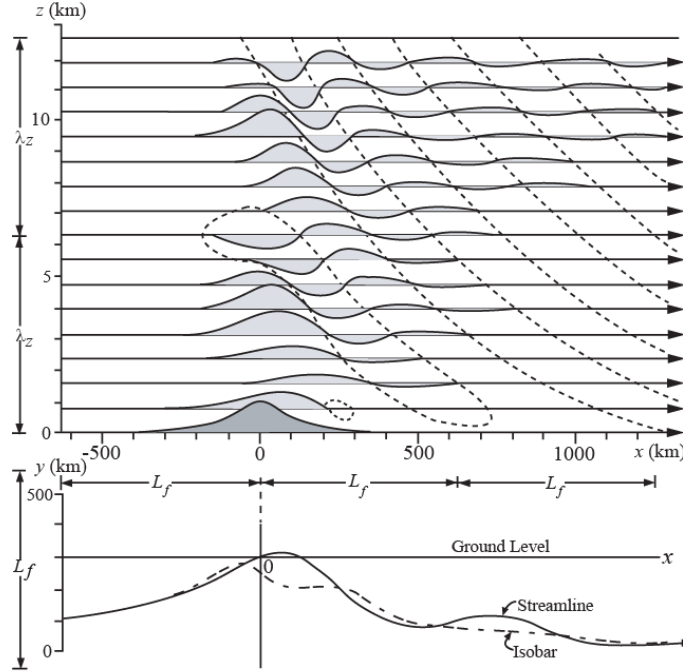


Fig. 5.27: Stratified rotating hydrostatic flow over a two-dimensional ridge with the parameters: $a = 100\text{km}$, $f = 10^{-4}\text{s}^{-1}$, $U = 10\text{ms}^{-1}$, and $N = 0.01\text{s}^{-1}$. Equation (5.5.2) multiplied by the non-Boussinesq factor $\sqrt{\rho_o / \rho(z)}$ is solved with an asymptotic method. This flow belongs to an intermediate regime between the nonrotating flow regime (e.g., Fig. 5.3b) and the quasi-geostrophic flow regime (e.g., Fig. 5.26a). The vertical wavelength of the wave is $\lambda_z \approx 2\pi U / N \approx 6.28\text{km}$. The bottom figure depicts the lateral deflection of the streamlines. In the figure, $L_f \approx 2\pi U / f \approx 600\text{km}$ near the surface. (Adapted after Queney 1948)

This flow belongs to an *intermediate or mesoscale mountain wave regime* between the *nonrotating flow regime* (e.g., Fig. 5.3b) and the *quasi-geostrophic flow regime* (e.g., Fig. 5.26a).

In this *intermediate regime* with $U/a \approx f$, both the *inertia force* and *Coriolis force* play comparable roles in generating and maintaining the mesoscale mountain waves.

The influence of the Coriolis force is evident in the lateral deflection of the streamlines and in the *dispersive tail of the longer waves trailing*

behind the mountain at upper levels. The horizontal wavelength is $L_f \approx 2\pi U/f \approx 600 \text{ km}$ near the surface and the vertical wavelength is $\lambda_z \approx 2\pi U/N \approx 6.28 \text{ km}$.

Unlike nonrotating flows, the upstream blocked decelerated zone produced by a mountain ridge on a uniform, stratified flow on an f plane does not propagate to infinity (Pierrehumbert and Wyman 1985). Instead, it attains a maximum extent on the order of the *Rossby radius of deformation* (Nh/f).

- Some rotational effects on three-dimensional stratified airflow past an isolated, mesoscale mountain are illustrated in Fig. 5.28.

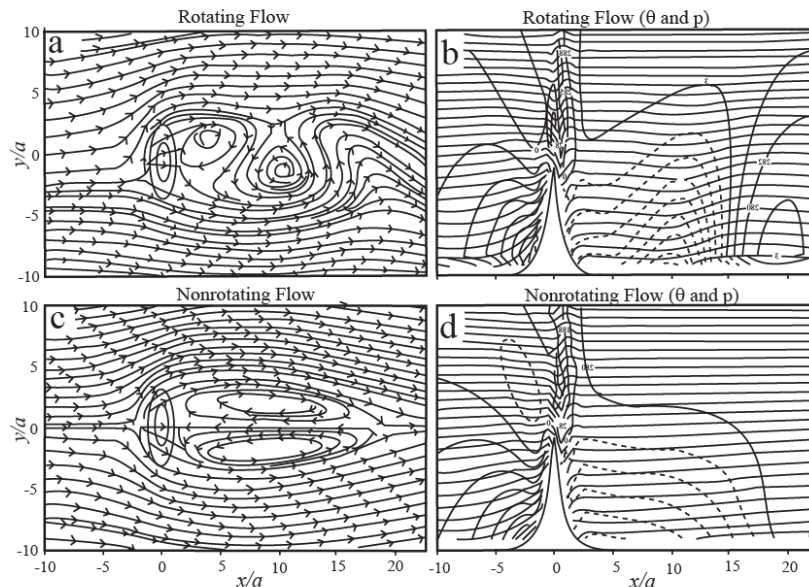


Fig. 5.28: (a) Surface streamlines, and (b) vertical cross section of potential temperature (horizontal curves) and pressure perturbations at the centerline ($y/a = 0$) for a uniform westerly flow over idealized topography after a non-dimensional time $Ut/a = 40$. The Froude number and the Rossby number are 0.4 and 2.15, respectively. The dimensional values of the flow and orographic parameters are: $U = 10 \text{ ms}^{-1}$, $f = 5.8 \times 10^{-5} \text{ s}^{-1}$, $a = 40 \text{ km}$, and $h = 2.5 \text{ km}$. In estimating the Rossby number, $2a$ is used. Panels (c) and (d) are the same as (a) and (b) except with no rotation. The x and y scales are non-dimensionalized by the mountain half-width in the x direction. (Lin 2007, Adapted after Lin et al. 1999)

With rotation, a significant portion of the upstream fluid particles move leftward (facing downstream) in response to the excessive pressure gradient force versus the reduced Coriolis force because the weakened easterly flow is out of balance geostrophically (Fig. 5.28a), compared with the case without rotation (Fig. 5.28c).

The separation point is shifted to the right-hand side in the rotating flow (Fig. 5.28a), instead of located along the centerline ($y/a = 0$) (Fig. 5.28c).

Downstream of the mountain, vortex shedding occurs. Over the mountain peak, the hydrostatic mountain wave is very weak because most of the flow is blocked by the high mountain and is deflected to the right or left, instead of climbing up and passing over the mountain (Fig. 5.28b).

On the cross section along the centerline ($y/a = 0$), both rotating and nonrotating flow produce blocking, high pressure and cold air over the upslope and low pressure and warm air over the downslope (Figs. 5.28b and 5.28d).

A southerly *barrier jet* forms along the upslope through geostrophic adjustment (see Ch. 1) in response to this reversed (against the basic flow) pressure gradient force in a rotating atmosphere (Fig. 5.28a).

In contrast, there is no barrier jet in a nonrotating flow (Fig. 5.28c). Due to the strong shear flow passing over the left tip of the mountain, a *jet* forms through the *corner effect* caused by the *Bernoulli effect* (Figs. 5.28a and 5.28c).

In the absence of rotation (Figs. 5.28c), a pair of cyclonic and anticyclonic vortices is generated on the lee, but these are symmetric with respect to the centerline.

The **vortex shedding** in a rotating flow also produces pressure and potential temperature perturbations far downstream (Fig. 5.28b). Three-dimensional flow past an isolated mountain in a rotating frame of reference has also been simulated using many other nonlinear numerical models.

- In addition to the above rotational effects, ***topographic Rossby waves*** can be produced for a flow over a mesoscale mountain.

To understand the **topographic Rossby waves**, one may consider an air column in a barotropic atmosphere that is pushed up northward against a sloping surface of an east-west oriented mountain range.

The air column tends to acquire an anticyclonic vorticity ($\zeta < 0$) in order to conserve the potential vorticity ($\approx (\zeta + f)/H$), where H is the effective depth of the air column, due to decreasing H .

An air parcel in the air column then turns anticyclonically, assuming f remains constant and the surface friction is negligible, and moves downslope. This forces the air column to stretch, thus acquiring cyclonic vorticity due to increasing H , and turn upslope.

This wavelike motion is called a **topographic Rossby wave** because the sloping surface plays an analogous role to that of the β effect.

By the way, what is “vortex Rossby waves”?

The PV generation in an inviscid fluid may be written as ([Mongomery and Enagonio 1998 JAS](#))

$$\frac{DQ}{Dt} = \frac{\zeta_a \cdot \nabla \theta}{\rho},$$

where Q is PV. In QG Boussinesq fluid,

$$\frac{DQ}{Dt} \approx \frac{(f + \zeta)}{\rho} \frac{\partial \theta}{\partial z}. \quad (7)$$

The main vortex's PV can be estimated similarly:

$$PV_{\text{main vortex}} \approx \frac{(f + \zeta)}{\rho} \frac{\partial \theta_{\text{total}}}{\partial z} \approx \frac{2f\theta_0 N^2}{g\rho} \approx 0.3 \text{ PVU}.$$

11.2 Lee cyclogenesis

The lee sides of mesoscale or large-scale mountains, such as the Alps, Rocky Mountains, the East Asian mountains and the Andes, are favorable regions of *cyclogenesis*.

This type of cyclogenesis is known as *lee cyclogenesis*, and can be defined as the formation of a cyclone with strong positive vertical vorticity or an appreciable fall in pressure with a closed circulation formed in the lee of a mountain that then drifts away.

Figure 5.29 shows the cyclogenesis frequency in the Northern Hemisphere during wintertime from 1899 to 1939.

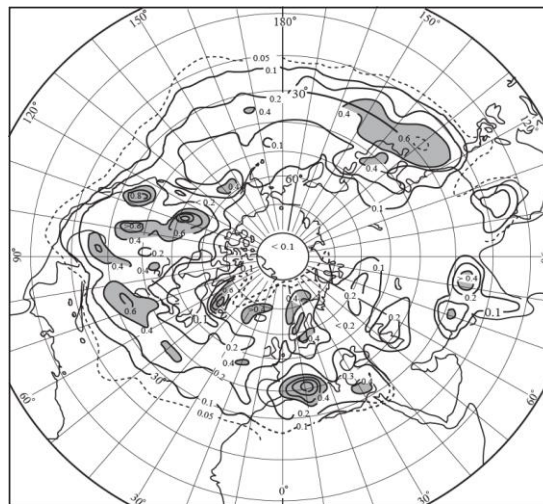


Fig. 5.29: Percentage frequency of cyclogenesis during winter from 1899 to 1939 in the Northern Hemisphere in squares of 100,000 km². (Adapted after Petterssen 1956)

Frequency maxima in the figure are located to the lee of major mountain ranges, such as south of the Alps over the Gulf of Genoa and to the east of the Rockies.

Similar to diabatic or differential heating, major mountain ranges serve as sources of stationary wave trains, which produce strong baroclinic zones favorable for *storm tracks* (Blackmon et al. 1977).

Two well-known storm tracks, the *Pacific trough* and the *Atlantic trough*, are associated with stationary, Rossby wave trains emanating from the *Himalayas and Rockies*, respectively.

Based on the above definition of lee cyclogenesis, the *weak stationary low* (pressure depression) associated with these stationary Rossby wave trains in the lee of mountains should be distinguished from the *true* lee cyclogenesis (Chung et al. 1976).

Observations indicate that lee cyclogenesis may be influenced by different factors, such as the synoptic conditions, as well as the orientation and geometry of the mountain range to the prevailing wind.

For example, the *Alps* are more isolated and parallel to the baroclinic flow, while the *Rockies* are more elongated and normal to the baroclinic flow.

In the following, we will focus the discussion on the theories of lee cyclogenesis over two major mesoscale mountain ranges, the Alps and Rockies. These theories can be applied to lee cyclogenesis over a number of mountain ranges in other parts of the world, depending upon the synoptic conditions and terrain geometry.

a. Alpine lee cyclogenesis

As depicted in Fig. 5.29, a frequency maximum of lee cyclogenesis can be found to the south of the Alps over the Mediterranean Sea.

Lee cyclogenesis over the Alps has been studied extensively, compared to that over other mountain ranges, partially due to the Alpine Experiment (ALPEX) field project held in 1982. The *general characteristics of the Alpine lee cyclogenesis* can be summarized as follows (e.g., Tibaldi et al. 1990):

- (a) Lee cyclogenesis often occurs in association with a preexisting synoptic-scale trough or cyclone that interacts with the orography;
- (b) The development of the lee cyclone starts before the strong thermal contrasts associated with cold frontal penetration take place in the lee;
- (c) The scales of mature and deep lee cyclones are on the order of the Rossby radius of deformation (NL_z/f , where L_z is the vertical scale of motion). The influence of orography takes the form of a high-low dipole, which has the same horizontal and vertical scales of the cyclone; and
- (d) A two-phase deepening process is found:
 - (i) In the first phase, the cyclone deepens very rapidly, but is shallow.
 - (ii) In the second phase, the cyclone develops less rapidly, but extends through the whole troposphere with horizontal scales comparable to the Rossby radius of deformation.

Based on upper-level flow, two types of lee cyclogenesis over the Alps can be identified: the *southwesterly flow (Vorderseiten) type* and the *northwesterly flow (Überströmungs) type* (Pichler and Steinacker 1987).

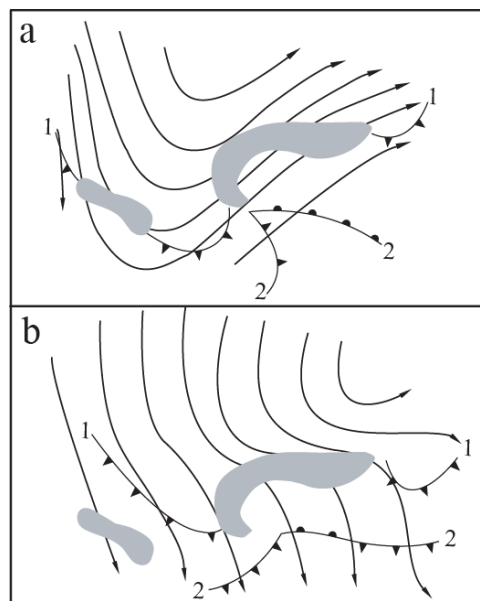


Fig. 5.30: Two types of lee cyclogenesis over the Alps: (a) **Southwesterly (Vorderseiten) type**, and (b) **Northwesterly (Überströmungs) type**, based on upper-level flow. The bold, solid lines indicate the upper-level flow and the surface fronts are plotted for two consecutive times, as denoted by 1 and 2. The shaded areas represent the terrain higher than 1 km. The mountains on the right hand side are the Alps and those on the left are the Pyrenees. (Lin 2007, Adapted after Pichler and Steinacker 1987)

- **Both types are accompanied by blocking and splitting of low-level cold air by the Alps.**
- One part of the low-level cold air flows anticyclonically around the Eastern (Dinaric) Alps, often leading to a *bora (bura)* event over the Adriatic Sea, while another part of the cold air flows around the Alps cyclonically and leads to the *mistral wind*, blowing through the Rhone Valley towards the Gulf of Lyons (to the south of France).
- **For the southwesterly type (Fig. 5.30a), cyclogenesis starts with the advance of an eastward moving trough, where a wave at the corresponding surface cold front** always forms in about the same place, i.e. the Gulf of Genoa (to the south of Italy and north of Corsica), due to the blocking and flow splitting effect of the Alps. A warm front is often generated over northern Italy.
- **For the northwesterly type (Fig. 5.30b), the upper-level flow blows generally from the northwest, which crosses the Alps and generates a cyclone on the lee.** The wave formation in the surface cold front occurs predominantly in the Gulf of Genoa, the same location as for the southwesterly type, due to the shape of the Alpine mountains.

A short wave trough embedded in the general northwesterly flow can, however, produce an intermediate southerly flow component. In the northwesterly type of lee cyclogenesis, there is no new cyclone formed in the lee of the Alps. Usually, there is a preexisting “parent” cyclone upstream northwest of the Alps, which is weakened by the anticyclone on the windward side of the Alps and intensified in the lee in a favorable baroclinic flow.

➤ There are two major theories for Alpine lee cyclogenesis have been proposed in the past:

- (1) Baroclinic lee waves (Smith 1984)
- (2) Orographic modification of baroclinic instability (Speranza et al. 1985)

As can be seen from the following description, it appears that the first mechanism is more applicable to the southwesterly type, while the second mechanism is more applicable to the northwesterly type.

- (1) The basic dynamics of the *baroclinic lee wave theory* can be understood by considering a quasi-geostrophic flow with an idealized, linear shear over an isolated mountain.

The basic wind represents an incoming cold front or baroclinic zone (with cold air to the west), similar to the southwesterly type (Fig. 5.30a; also see Fig. 1 of Lin and Perkey (1989)).

This basic wind profile allows for the growth of a standing baroclinic wave in the lee (south) of the mountain. Although a *baroclinic wave* is often used to imply a growing, baroclinically unstable wave, here we define it more generally as a surface-trapped wave in a baroclinic current whose restoring force is associated with temperature advection at the boundary. Based on the quasi-geostrophic approximation, the geostrophic, Boussinesq potential vorticity equation on an f -plane can be written as (Smith 1984):

$$\frac{D_g}{Dt} \left(\nabla^2 P + \frac{f^2}{N^2} P_{zz} \right) = 0, \quad (5.5.6)$$

where P is the pressure, the terms inside the bracket are the potential vorticity, $D_g / Dt = \partial / \partial t + u_g \partial / \partial x + v_g \partial / \partial y$, $u_g = -P_y / (\rho_o f)$, $v_g = P_x / (\rho_o f)$, and the thermodynamic equation at the surface is,

$$\frac{D_g \theta}{Dt} + w \frac{\partial \theta}{\partial z} = 0, \text{ at } z = 0, \quad (5.5.7)$$

where θ is the potential temperature. Assuming $u_g = U(z) + u_g'$ and $v_g = V(z) + v_g'$ and the basic flow velocity is a linear function of height, i.e. $U(z) = U_s + U_z z$ and $V(z) = V_s + V_z z$, then the potential vorticity in (5.5.6) vanishes everywhere. Here U_o and V_o are the basic wind speeds at surface. Thus, any perturbation to this basic state must obey,

$$\nabla^2 p' + \frac{f^2}{N^2} p'_{zz} = 0 \quad (5.5.8)$$

and

$$\left(\frac{\partial}{\partial t} + U_s \frac{\partial}{\partial x} + V_s \frac{\partial}{\partial y} \right) \frac{\partial p'}{\partial z} - U_z \frac{\partial p'}{\partial x} - V_z \frac{\partial p'}{\partial y} + \rho_o N^2 w' = 0 \text{ at } z = 0, \quad (5.5.9)$$

where $N^2 = (g / \theta_o)(\partial \bar{\theta} / \partial z)$. The above two equations form a closed system as long as w' is known at $z = 0$, which can be specified by the linear lower boundary condition, $w'(x, y, z = 0) = U_s \partial h / \partial x + V_s \partial h / \partial y$, where $h(x, y)$ is the mountain height function.

If one considers a two-dimensional, steady-state flow over a bell-shaped mountain ridge, $h(x) = ha^2 / (x^2 + a^2)$, an analytical solution can be obtained by applying the Fourier transform to both (5.5.8) and (5.5.9) and an upper boundedness boundary condition (which differs from the rigid lid boundary condition) in a semi-infinite vertical plane.

The solution can be written as

$$p'(x, z) = \rho_o U_s N^2 \left[2 \operatorname{Re} \int_0^\infty \frac{\hat{h}(k) e^{-z/H} e^{ikx}}{U_s / H + U_z} dk \right], \quad (5.5.10)$$

where $H(k) = f / Nk$ and $\hat{h}(k) = (ha/2)e^{-kx}$. In deriving (5.5.10), we have applied the one-sided Fourier transform. According to the Riemann-Lebesgue Lemma (Appendix 5.1), the integral will go to 0 as $|x| \rightarrow \infty$ due to the rapid oscillation of the term e^{ikx} . In this case, the airflow will be disturbed only near the mountain.

However, if the denominator of the integrand vanishes for some value of k , the integral will not vanish. This happens when there is a back shear. For example, when $U_s > 0$, this requires $U_z < 0$ and the basic wind vanishes at height $H^* = f / Nk^*$ (where $k^* = NH^* / f$ and H^* is the wind reversal level).

Thus, the vanishing of the basic wind $U(z)$ at some height is the condition for obtaining a disturbance away from the mountain. Physically, this is an orographically-forced standing baroclinic wave which has a zero phase speed.

Evaluating (5.5.10) gives

$$p'(x, z) = 0, \quad \text{for } x < 0 \quad \text{and} \quad (5.5.11a)$$

$$p'(x, z) = -(4\pi\rho_o Nf)\hat{h}(k^*)e^{-z/H^*} \sin k^* x \quad \text{for } x > 0. \quad (5.5.11b)$$

Equation (5.5.11b) describes a train of standing baroclinic lee waves on the lee of the mountain. With typical flow and orographic parameters for Alpine lee cyclogenesis, such as $\rho_o = 1 \text{ kg m}^{-3}$, $N = 0.01 \text{ s}^{-1}$, $f = 10^{-4} \text{ s}^{-1}$, $h = 3 \times 10^3 \text{ m}$, $a = 2.5 \times 10^5 \text{ m}$, $H^* = 5 \times 10^3 \text{ m}$, and $k^* = f/(NH^*) = 2 \times 10^{-6} \text{ m}^{-1}$, a pressure perturbation $p' = 28 \text{ hPa}$ can be generated.

The wavelength of the baroclinic lee wave is $\lambda = 2\pi/k^* \approx 3000 \text{ km}$, which is comparable to observed baroclinic waves over the Alps.

To obtain the transient solution, we take the Fourier transform of (5.5.8), applying the upper boundedness boundary condition, and then substitute the solution to (5.5.9) with the linear lower boundary condition. This leads to

$$\hat{p}(t) = Ae^{-Bt} + \frac{Hg\rho_o\bar{\theta}_z}{\theta_o} \frac{ikU_s\hat{h}}{B}, \quad (5.5.12)$$

where

$$B = ik(U_s + HU_z), \quad (5.5.13)$$

and A is a complex coefficient to be determined by the initial condition. The solution in physical space can then be obtained by taking the inverse Fourier transform of (5.5.12). One can apply a FFT algorithm to obtain the numerical solution.

Figure 5.31 shows examples of the steady-state solution, (5.5.11), and the transient solution of (5.5.12) with an initially undisturbed flow, $p'(t = 0) = 0$.

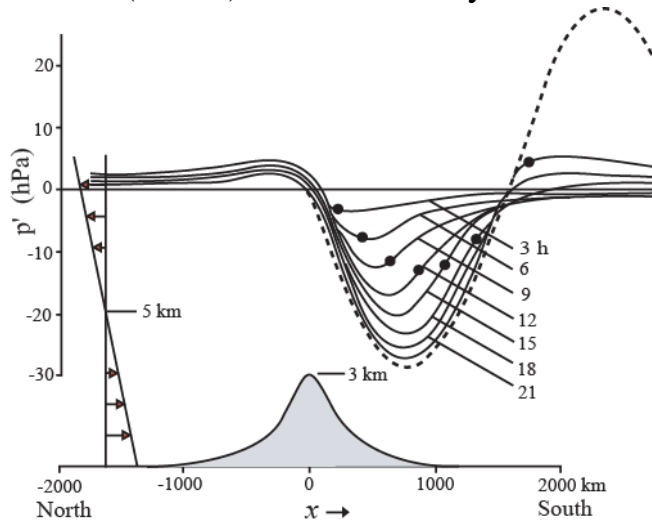


Fig. 5.31: Baroclinic lee wave theory of lee cyclogenesis: an example of the steady-state solution (dashed curve), (5.5.11), and transient solution (solid

curves), (5.5.12) for an initially undisturbed, back-sheared flow over a bell-shaped mountain, $h(x) = ha^2 / (x^2 + a^2)$. The flow and orographic parameters are: $\rho_o = 1 \text{ kg m}^{-3}$, $N = 0.01 \text{ s}^{-1}$, $f = 10^{-4} \text{ s}^{-1}$, $h = 3 \text{ km}$, $a = 2.5 \times 10^5 \text{ m}$, $U_s = 20 \text{ ms}^{-1}$ and $H^* = 5 \times 10^3 \text{ m}$. (Adapted after Smith 1984)

This leads to rapid lee cyclogenesis with pressure tendencies from 4 to 6 mb/3h. The fluid is, in effect, trying to form the first trough of a standing baroclinic lee wave.

Compared with the steady state solution, the transient solution produces the simple pattern of a wave growing away from its source.

The above system has been extended to obtain the following (Smith 1986):

- (a) Three-dimensional numerical solutions for Alpine cyclogenesis, which show qualitative agreement with observations;
- (b) An upshear phase tilt with height which indicates that the growing baroclinic wave is able to extract energy from the available potential energy stored in the baroclinic shear flow;
- (c) With a rigid lid added to the model, there is a rapid two-phase lee cyclone growth supported by baroclinic instability of the Eady type (1949);
- (d) The baroclinic lee waves belong to the regime of mixed inertia-gravity waves and trapped baroclinic lee waves (Sec. 3.8), thus making the theory more applicable to flow with moderate Ro and moderate Ri , or small Ro and moderate Ri ; and (e) the basic features predicted by the linear theory are consistent with those simulated by nonlinear numerical models (Lin and Perkey 1989; Schär 1990).

(2) *Orographic modification of baroclinic instability*

In this theory, the formation of Alpine lee cyclogenesis is attributed to the baroclinically unstable modes modified by orography.

To derive the governing equations, we assume a small-amplitude mountain and a basic flow with constant stratification and vertical shear, and a zonal wind that vanishes at $z=0$, bounded between $z=0$ and $z=H$ in the vertical and by lateral walls at $y = \pm L_y / 2$. For this type of flow, the linear, nondimensional governing equations and boundary conditions can be written as (Speranza et al. 1985):

$$\begin{aligned}
\nabla^2 \psi + \psi_{zz} &= 0, \\
\psi_{zt} - \psi_x &= -J_{yz}(\psi, h/R_o) \quad \text{at } z=0, \\
\psi_{zt} - \psi_x + \psi_{xz} &= 0 \quad \text{at } z=1, \text{ and} \\
\psi &= 0 \quad \text{at } y = \pm L_y/2,
\end{aligned} \tag{5.5.14}$$

where ψ is the streamfunction, J the Jacobian [defined as $J_{yz}(\alpha, \beta) = \alpha_y \beta_z - \beta_y \alpha_z$], h the mountain height, and R_o the Rossby number. Note that (5.5.14) is equivalent to (5.5.8) of the baroclinic lee wave theory except that the streamfunction is used. Assuming $\psi(t, x, y, z) = \phi(x, y, z)e^{-i\omega t}$ and applying the Fourier series expansion to the above system reduces it to an eigenvalue problem, which allows one to find the most unstable baroclinic wave mode from the eigenvalues.

Figure 5.32 shows one example of Alpine lee cyclogenesis based on the above theory.

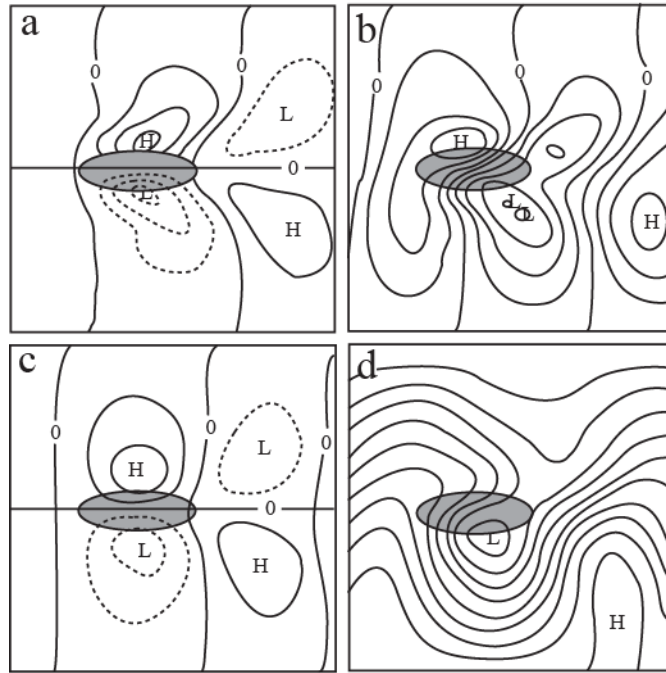


Fig. 5.32: Orographic modification of baroclinic instability for Alpine lee cyclogenesis: An example of cyclogenesis generated by a baroclinic wave in the continuous Eady model, in a long periodic channel with isolated orography. The mountain has a bi-Gaussian form ($e^{-x^2/a^2} e^{-y^2/b^2}$) and the dimensional values of a and b are 1500 km and 500 km, respectively. The shaded oval denotes the orographic contour of e^{-1} of the maximum height. (a) Streamfunction of

orographic perturbation at $z = 0$ (nondimensional); (b) total streamfunction of the modified baroclinic wave at $z = 0$; (c) and (d) are as (a) and (b), respectively, but at the middle level, $z = 0.5$. The basic zonal wind is added in (d). (Lin 2007, Adapted after Speranza et al. 1985)

The disturbance at the surface (Figs. 5.32a and 5.32b) is more localized near the mountain than that at the mid-troposphere (Figs. 5.32c and 5.32d). The total streamfunction fields (Figs. 5.32b and 5.32d) appear to be able to capture some basic structures of Alpine lee cyclones in the mature stage. Lee cyclogenesis is explained as the intensification of the incident baroclinic wave taking place on the southern (warm) side of the mountain, together with a weakening of the wave amplitude on the northern (cold) side.

When a vertical wall is used to represent the Alps and to block all meridional flow below the crest level, a lee cyclone develops through baroclinic instability (Egger 1972; Pierrehumbert 1986), as in Fig. 5.32, and so the situation illustrated in Fig. 5.32 may thus be considered to belong to the mechanism of orographic modification of baroclinic instability. In fact, the above two theories for Alpine lee cyclogenesis are related because both of them are built upon the baroclinic instability theory of Eady (1949), as can be seen from (5.5.8) and (5.5.14), but use different initial and upper boundary conditions and basic wind profiles.

In the baroclinic lee wave theory, an undisturbed flow or a localized baroclinic wave is used to initiate the process, while a fully-developed baroclinic wave is used as the initial condition in the theory of orographic modification of baroclinic instability. In addition, the theory of orographic modification of baroclinic instability uses a rigid lid upper boundary condition, as in Eady's model, while the baroclinic lee wave theory does not impose a rigid lid but uses a back-sheared north-south basic wind profile.

Based on the above discussions, it appears that the baroclinic lee wave mechanism is more applicable to the southwesterly cyclogenesis type, while the mechanism of orographic modification of baroclinic instability is more applicable to the northwesterly type which normally contains a preexisting cyclone.

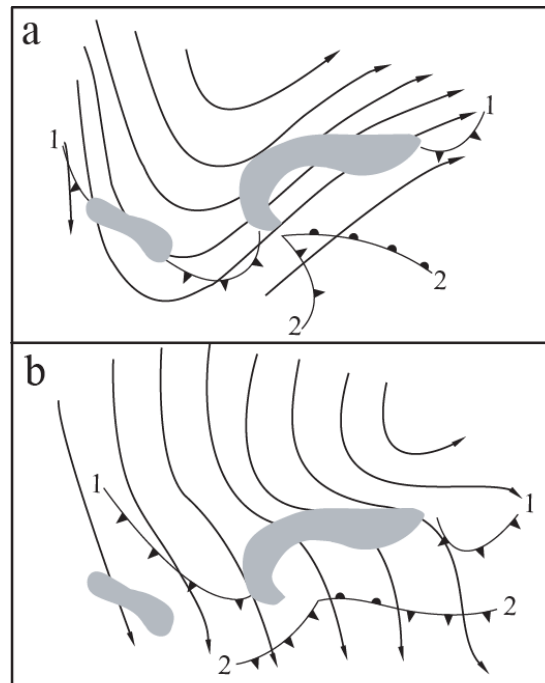


Fig. 5.30: Two types of lee cyclogenesis over the Alps: (a) **Southwesterly (Vorderseiten) type**, and (b) **Northwesterly (Überströmungs) type**, based on upper-level flow. The bold, solid lines indicate the upper-level flow and the surface fronts are plotted for two consecutive times, as denoted by 1 and 2. The shaded areas represent the terrain higher than 1 km. The mountains on the right hand side are the Alps and those on the left are the Pyrenees. (Lin 2007, Adapted after Pichler and Steinacker 1987)

Some other physical processes may also play important roles in the Alpine lee cyclogenesis, such as nonlinear processes (Tafferter and Egger 1990), geostrophic adjustment to upper-level potential vorticity advection (Bleck and Mattock 1984), and orographic modification of the baroclinic parent cyclone (Orlanski and Gross 1994), under certain synoptic situations.

The two-phase deepening process has been attributed to the rapid formation of a low-level orographic vortex, followed by its baroclinic and diabatic interaction with an approaching upper-level trough (Aebischer and Schär 1998).

In the first phase, orographically generated elongated bands of positive and negative PV, i.e. *PV banners or streamers*, may wrap up and subsequently contribute to the low-level PV anomaly within the developing cyclone. The second phase is interpreted as mere orographic modification of baroclinic instability.

b. Rockies lee cyclogenesis

The major difference that sets apart the Rockies lee cyclogenesis from the Alpine lee cyclogenesis is that **the Rocky Mountains are elongated in a direction normal to the basic wind, while the Alps are elongated in a direction parallel to the thermal wind (basic wind shear).**

In addition, the Rocky Mountains have a much larger horizontal scale than the Alps in the direction of the low-level flow. Three stages can be identified for the lee cyclogenesis over the Rocky Mountain cordillera:

- (a) **Stage I:** A **parent cyclone** approaches the Rocky Mountain cordillera from the northwest. As the cyclone moves closer to the mountains, it **decelerates and curves to the north.**
- (b) **Stage II:** During the passage of the parent cyclone over the cordillera, **the low-level portion of the cyclone weakens or fills in (disappears) over the mountain, while the upper-level trough continues to move over the mountain, but with some track deflection;**
- (c) **Stage III:** A **new surface cyclone forms in the lee of the mountain range and to the south of the original track.** In the meantime, an upper-level trough, which is associated with the parent cyclone, has progressed over the mountain and helps strengthen the surface cyclone through baroclinic development.

Figure 5.33 shows an example of cyclogenesis which occurred in the lee of the U.S. Rocky Mountain cordillera on 18-20 March 1994.

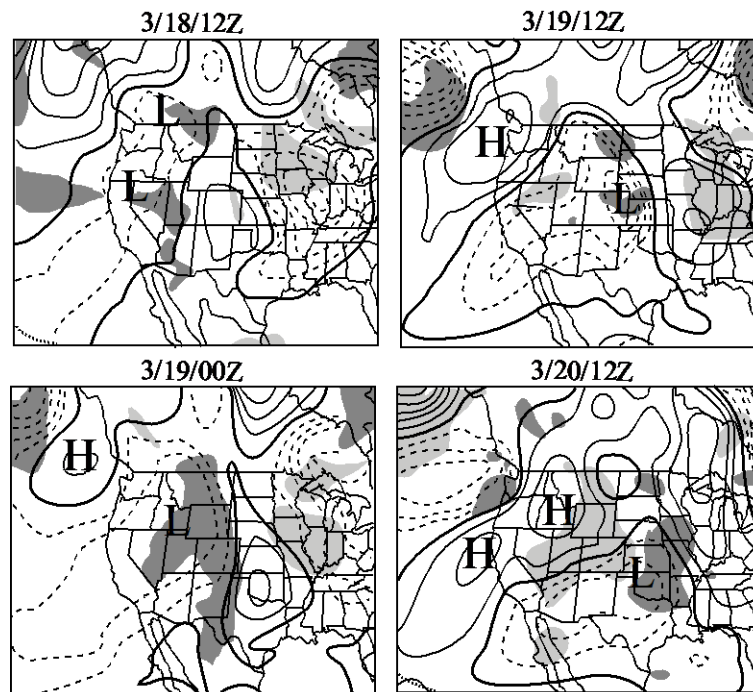


Fig. 5.33: An example of Rockies lee cyclogenesis. Three stages, as summarized in the text, are clearly shown in the perturbation geopotential fields on 860 mb at 12-h intervals from 3/18/12Z (1200 UTC 18 March) to 3/20/12Z 1994. Solid (Dashed) contours denote positive (negative) values, while bold solid contours denote zero geopotential perturbations. Darker (Lighter) shading denotes warm (cold) areas at 900-mb $\theta' \geq 4$ K ($\theta' < 4$ K). (Lin 2007, Adapted after Davis 1997)

At 1200 UTC 18 March (3/18/12Z), a parent cyclone was located over the southern Oregon and was approaching the Rockies. It subsequently moved eastward over southern Idaho by 3/19/00Z (Stage I).

Stage II occurs between 3/19/00Z and 3/19/12Z. At 3/19/12Z, a new cyclone forms over eastern Colorado, which is to the southeast of the incidence of the parent cyclone. As the upper-level trough begins moving east of the mountains, the phase shift between the upper trough and the lee cyclone begins to decrease and classical baroclinic development takes place.

Similar to Alpine lee cyclogenesis, the Rockies lee cyclogenesis has also been studied extensively in the past and several mechanisms have been proposed.

Due to the fact that a parent cyclone is almost a prerequisite for the Rockies lee cyclogenesis and that the flow is highly baroclinic, [the formation of lee cyclones can be reasonably explained by the theory of orographic modification of baroclinic instability, described by \(5.5.14\).](#)

The major difference is that the low-level tracks of the Rocky Mountains cyclones are strongly influenced by the mountain geometry, as will be discussed in subsection 5.5.3, and by the upper-level trough's effect on the intensity of the lee cyclone.

The theory of orographic modification of baroclinic instability, as described in (5.5.14), can be extended to avoid the limitations of gentle sloping and small amplitude mountains by allowing for the interaction of growing normal modes in a baroclinic channel with isolated topography of finite height (Buzzi et al. 1987).

In addition, the isolated mountain may be elongated in the north-south direction to mimic the Rockies topography. Figure 5.34 shows the time evolution of the fastest growing baroclinic mode in the lower layer of the two-layer channel model.

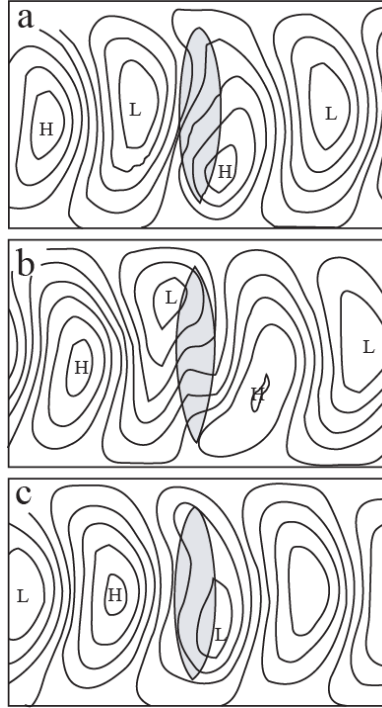


Fig. 5.34: Application of a linear theory of orographic modification of baroclinic instability to the Rockies lee cyclogenesis. The streamfunction of the fastest growing mode in the lower layer of a two-layer channel model on a β plane, at three times of evolution of the baroclinic mode are shown, which also reflects the three stages of Rockies lee cyclogenesis (see text). The channel length and width are 10000 and 6000 km, respectively. The basic state mean velocity is 17 ms^{-1} in the upper layer and 0 ms^{-1} in the lower layer. The area of the mountain with height above he^{-1} is shaded, where h is the mountain height (2.5 km). (Adapted after Buzzi et al. 1987)

The three stages summarized earlier are reasonably reproduced by this linear stability model. The track deflection will be explained in Subsection 5.5.3.

Note that nonlinearity should be included in the above lee cyclogenesis theory when applied to the real atmosphere (Tafferter and Egger 1990). Various physical processes have been emphasized in other theories of the orographic modification of baroclinic instability mechanism, such as: (1) superposition of a growing baroclinic wave and a steady mountain wave (e.g., Hayes et al. 1993), and (2) Eady edge waves, i.e., an orographically modified surface potential temperature distribution

leading to the upstream northward deviation of the baroclinic waves (Davis 1997).

c. Mesoscale lee cyclogenesis

A mesoscale vortex formed on the lee of a mesoscale mountain, as discussed in the subsection 5.4.2, can further develop into a lee cyclone by acquiring low pressure at the center of the vortex through various processes, such as latent heating associated with moist convection, surface heating over a warm sea surface, merging with a nearby mesolow, and interaction with an approaching upper-level trough. This type of mesoscale cyclogenesis has been observed in the lee of some mesoscale mountains and simulated by numerical models.

Examples are the

- [Denver cyclone](#) (Crook et al. 1990),
- [Mesocyclones generated to the east of Taiwan's CMR](#) (Sun et al. 1991; Lin et al. 1992), and
- [Lee cyclones generated by the northern Korean mountain complex over the East \(Japan\) Sea](#) (Lee et al. 1998).

11.3 Orographic influence on cyclone track

Similar to what is shown in Fig. 5.33, track deflection of cyclones by mountains also occurs in other mesoscale mountain ranges, such as the Appalachians and Greenland, as long as the mountain range has appreciable extension in the direction normal to the prevailing wind in which the cyclone is embedded. Orographic influence on cyclone tracks has also been observed for tropical cyclones passing over mesoscale mountains, such as the northern Philippines and the Caribbean Islands, the Sierra Madre of Mexico, and Taiwan.

[Figure 5.35](#) shows examples of track deflection of tropical cyclones past the CMR of Taiwan. Depending upon the intensity, steering wind

speed, size of the cyclone, landfalling location and impinging angle, the tracks over CMR can be classified as continuous or discontinuous.

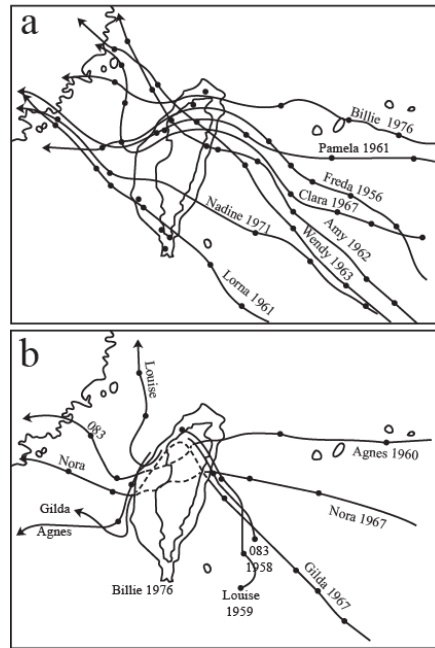


Fig. 5.35: Tropical cyclones traversing the Central Mountain Range (CMR) of Taiwan with (a) continuous tracks, and (b) discontinuous tracks. A cyclone track is defined as discontinuous when the original cyclone (i.e. a low pressure and closed cyclonic circulation) and a lee cyclone simultaneously co-exist. (Adapted after Wang 1980 and Chang 1982)

Figure 5.36 illustrates the orographic influence on cyclone track through the turning of the basic flow and the outer circulation of the cyclone.

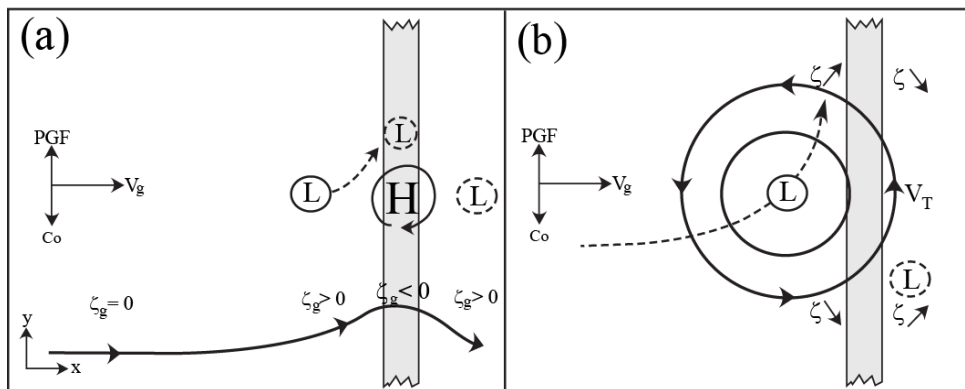


Fig. 5.36: Effects of shallow orography on cyclone track deflection through the turning of (a) the basic flow and (b) outer circulation of the cyclone. The solid-circled L and dash-circled L denote the parent and new cyclones, respectively. The incoming flow is geostrophically balanced. H denotes the mountain-induced high pressure. The lower curve in (a) denotes the trajectory of an upstream air parcel. The cyclone is steered to the northeast by the basic flow velocity \mathbf{V}_g . ζ_g is the vertical vorticity associated with the basic flow. In (b), the dashed curve associated with L denotes the cyclone track. The new cyclone forms on the lee due to vorticity stretching associated with the cyclonic circulation that is, in turn, associated with the parent cyclone. V_T is the characteristic tangential wind speed of the parent cyclone, such as the maximum tangential wind (V_{\max}). The arrow adjacent to ζ denotes the local vorticity tendency ($\partial\zeta/\partial t$). (Panel (b) is adapted after Carlson 1998)

The orography is assumed to be shallow, so that the blocking is relatively weak and most of the low-level air is able to pass over the mountain. The track deflection of a cyclone embedded in a straight incoming flow on a mesoscale mountain ridge, as shown in Fig. 5.36a, can be explained by either the force balance or the conservation of potential vorticity, as discussed earlier along with Fig. 5.26a.

Cyclone tracks can also be affected by the orographic influence on the outer circulation of the cyclone. This process is illustrated in Fig. 5.36b. Air ascends in the southwest and northeast quadrants and descends in the northwest and southeast quadrants with respect to the intersection of the original (west-east) undisturbed track and the mountain crest.

This produces a positive local vorticity tendency ($\partial\zeta/\partial t > 0$) in the northwest and southeast quadrants due to vorticity stretching, $(\zeta + f)\partial w/\partial z$ (e.g., part of the second term on the right side of (5.4.28) with the Coriolis term added). Similarly, $\partial\zeta/\partial t < 0$ is produced in the southwest and northeast corners due to vorticity shrinking. This helps migrate the cyclone toward the northwest corner and generate a secondary (new) cyclone in the southeast quadrant.

The lee cyclone develops quickly once it is coupled with the upper portion of the parent cyclone or trough. Note that this process will produce a lee cyclone that is at most of the same strength as the parent

cyclone. In order to generate a stronger lee cyclone, other processes are required, such as barolinic instability or upstream flow blocking.

The continuity of cyclone tracks and degree of track deflection is directly related to the degree of orographic blocking. Figure 5.37 shows orographic influence on cyclone track deflection for a passive cyclone in a uniform flow past an isolated, finite-length mountain on an f -plane.

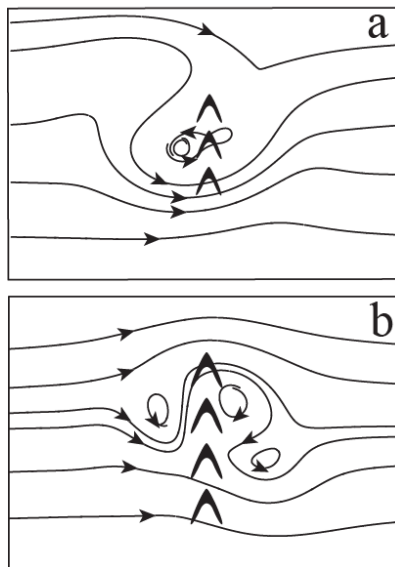


Fig. 5.37: Orographic influence on cyclone track deflection for a drifting cyclone in a uniform flow past an isolated, finite-length mountain (denoted by the mountain symbol) on an f -plane: (a) weak blocking, and (b) strong blocking. (Lin 2007, Adapted after Lin et al. 2005)

With weak blocking (panel a), the cyclone is deflected to the right (facing downstream) and a weak secondary cyclone forms on the lee. The track is continuous in this case.

With strong blocking (panel b), the cyclone is deflected to the left and a relatively strong secondary cyclone forms on the lee. In this case, the track is discontinuous. It is found that the track deflection is associated with the local vorticity tendency ($\partial\zeta/\partial t$) which is dominated by the vorticity advection and vorticity stretching while the cyclone is crossing over a mesoscale mountain range (Lin et al. 1999; 2005).

For example, for the case of Fig. 37a (weak blocking), the track deflection is dominated by vorticity advection. For the case of Fig. 37b, strong blocking tends to generate a strong northerly jet along the upwind slope of the mountain range, which, in turn, produces a local vorticity tendency to the left (north) of the undisturbed cyclone track by vorticity advection.

The strong secondary vortex on the lee is generated by the vorticity stretching. The degree of orographic blocking can be measured by nondimensional control parameters, such as the basic-flow Froude number (U/Nh), the vortex Froude number (V_T/Nh), and the relative scale of the cyclone and the orography in the direction perpendicular to the steering flow (R/L_y), where U is the basic flow speed, V_T the characteristic tangential wind speed of the parent cyclone (such as V_{\max}), N the Brunt-Vaisala frequency, h the mountain height, and R is the cyclone scale represented by its radius of maximum tangential wind.